Acta geographica Slovenica, 62-2, 2022, 23–47

SPATIOTEMPORAL EVOLUTION OF DROUGHTS AND THEIR TELECONNECTIONS WITH LARGE-SCALE CLIMATIC INDICES IN THE LOWER SEBOU BASIN IN NORTHWESTERN MOROCCO

Oualid Hakam, Abdennasser Baali, Khalil Azennoud, Touria El Kamel, Yassine Ait Brahim, Youssra Ahouach

OUALID HAKAM

Effects of drought on soils and rainfed crops (cereals).

DOI: https://doi.org/10.3986/AGS.10508
UDC: 551.577.38(64)
COBISS: 1.01

Oualid Hakam[1], Abdennasser Baali[1], Khalil Azennoud[1], Touria El Kamel, Yassine Ait Brahim[2], Youssra Ahouach[1]

Spatiotemporal evolution of droughts and their teleconnections with large-scale climatic indices in the Lower Sebou Basin in northwestern Morocco

ABSTRACT: The Lower Sebou Basin, placed in a Mediterranean climate, has the particularity of being exposed to the influence of disturbances from the Atlantic Ocean, making periods of drought and climatic phenomena variable in space and time. Applying the world's most recognized drought indices, shows that the duration, frequency and severity of droughts have increased since the start of the 21st century. These results revealed and placed in the even wider regional climatic context, including the two dominant atmospheric oscillations such as the North Atlantic Oscillation (NAO) and the Mediterranean Oscillation (MO), suggest that the significant drought trends determined are correlated with the relative facts of the two oscillations.

KEY WORDS: drought, teleconnection, Lower Sebou Basin, Morocco

Prostorsko–časovni razvoj suš in njihove povezave z obsežnimi podnebnimi indeksi v porečju Lower Sebou v severozahodnem Maroku

POVZETEK: Kotlina spodnjega Sebouja, kjer je sredozemsko podnebje, ima posebnost, da je izpostavljena vplivom motenj, ki prihajajo iznad Atlantskega oceana. Zaradi tega so obdobja suše in podnebnih pojavov spremenljiva v prostoru in času. Uporaba uveljavljenih svetovnih indeksov suše kaže, da so se trajanje, pogostost in intenzivnost suš od začetka 21. stoletja povečala. Doseženi rezultati, postavljeni tudi v širši regionalni podnebni kontekst, vključno z dvema prevladujočima atmosferskima nihanjema, kot sta severnoatlantsko nihanje (NAO) in sredozemsko nihanje (MO), kažejo, da so ugotovljeni pomembni trendi suše povezani z relativnimi dejstvi obeh nihanj.

KLJUČNE BESEDE: suša, klimatske povezave na daljavo, kotlina spodnjega Sebouja, Maroko

The article was submitted for publication on December 24th, 2021.
Uredništvo je prejelo prispevek 24. decembra 2021.

[1] Sidi Mohamed Ben Abdallah University, Faculty of Sciences Dhar El Mehraz, Laboratory of engineering, electrochemistry, modeling and environment, Fez, Morocco
oualid.hakam@gmail.com (https://orcid.org/0000-0001-6831-5365), baaliabdennasser@gmail.com, khalil.azennoud.fst@gmail.com (https://orcid.org/0000-0003-2539-394X), touria.elkamel@gmail.com (https://orcid.org/0000-0003-4508-2399), youssra.ahouach@gmail.com

[2] Mohamed VI Polytechnic University, International Water Research Institue, Ben Guerir, Morocco
aitbrahim.yassine@gmail.com (https://orcid.org/0000-0003-3098-7339)

1 Introduction

Drought is a climatic phenomenon considered to be one of the most loss–making natural disasters in the world and affects a large number of people each year. An estimated 55 million people globally are affected by droughts every year (Vatter, Wagnitz and Hernandez 2019; United Nations Office for Disaster Risk Reduction 2021). It occurs when there is less rainfall in an area for a long period or when there is a poor distribution of rainfall over some time. The American Meteorological Society has classified droughts into four types: meteorological drought, hydrological drought, agricultural drought and socio–economic drought (Yihdego, Vaheddoost and Al-Weshah 2019). They may not occur simultaneously, but meteorological drought remains the driving force behind the others (Wilhite 2006). This drought can take the form of permanent droughts, like what is occurring in arid and semi–arid or Mediterranean climates during the summer season or in subtropical regions in winter. As well as it may turn out to be a natural disaster when it becomes high frequency with longer duration. Therefore, the assessment and characterization of meteorological drought are most important to understand these risks. However, the assessment of drought characteristics and its spatial variability is still very difficult (Vicente-Serrano et al. 2020). For this purpose, many indices have been developed to identify and quantitatively characterize drought events, in order to monitor and predict the onset, termination and impacts of drought (Bayissa et al. 2018). On the other hand, no single index can represent all aspects of meteorological drought (Yihdego, Vaheddoost and Al-Weshah 2019). To overcome this constraint, a multi–index approach was adopted for the characterization of drought in the Lower Sebou Basin (LSB). As a result, two drought indices can be used as a basis for characterizing meteorological drought in the LSB, the Standardized Precipitation Index (SPI) (McKee, Doesken and Kleist 1993) and the Standardized Precipitation–Evapotranspiration Index (SPEI) (Vicente-Serrano, Beguería and López-Moreno 2010). Widely used in the world (Vicente-Serrano et al. 2012; Beguería et al. 2014; Šebenik, Brilly and Šraj 2017) and recommended by the World Meteorological Organization (World Meteorological Organization 2012), these indices have been recently applied in the LSB due to their performance and regional applicability compared to other drought indices (Hakam et al. 2022a). The SPI and SPEI approaches are similar, but there are obvious differences between the input parameters for the calculation. The SPI calculation requires rainfall data, and is well suited in time and space, but the SPEI uses the difference between rainfall and potential evapotranspiration (PET), which can account for the possible effects of temperature variability and temperature extremes beyond the context of global warming.

In Morocco, as the Mediterranean semi–arid areas, drought is one of the most frequent and widespread natural disasters and has become a structural element of the country's climate in recent decades, as shown by Stigter, Nunes and Pisani (2014) for case studies in south Portugal, Spain and Morocco. According to a recent study by Woillez (2019), rainfall in Morocco has generally decreased significantly over the period 1951–2010, between -10 and -25 mm per year in the north of the country, with temperature increases in the order of +1 °C to +2 °C on average annually between 1901 and 2012. Over the last 30 years, the trend is clearly higher than the global average, with + 0.42 °C per decade on average since 1990, compared to + 0.28 °C per decade on average on all continents (Woillez 2019), resulting in an increase in the frequency and intensity of extreme events such as drought and flooding. The LSB was not spared in recent decades and experienced heatwaves in 1995 and 2001 and floods in 1996, 2002 and 2009 (Agence du Bassin Hydraulique de Sebou 2010).

The spatio-temporal evolution of droughts in the LSB is controlled by landscape heterogeneity and specific climatic events such as extreme weather anomalies and large-scale atmospheric circulations (Lamb and Peppler 1987; Zamrane, Mahé and Laftouhi 2021; Hakam et al. 2022b). Some studies have demonstrated an anti–correlation of rainfall in Morocco, especially in the northwestern part, and the North Atlantic Oscillation (NAO) (Marchane et al. 2016; Driouech et al. 2021). Knowing that the calculation of this oscillation, which makes its effects felt in winter, is based on the difference in atmospheric pressure between the Icelandic low and the Azores high, neglecting the Mediterranean Oscillation (MO) despite the proximity of the Mediterranean Sea. Indeed, it has been shown that the MO index influences the seasonal variability of rainfall in the Mediterranean basin, especially in winter (Criado-Aldeanueva and Soto-Navarro 2020). Currently, drought studies in the LSB are scarce, most of them being based on simple statistical approaches (El Jihad, Peyrusaubes and El Bouzidi 2014; Acharki et al. 2019).

More vulnerable than other basins, facing numerous droughts (Ajlal and Agoutime 2021; Hakam et al. 2022a) and subject to a drought warning by the Regional Observatory of the Environment and Sustainable Development in Morocco (2014), the climatic study of the LSB has become paramount. As no regional

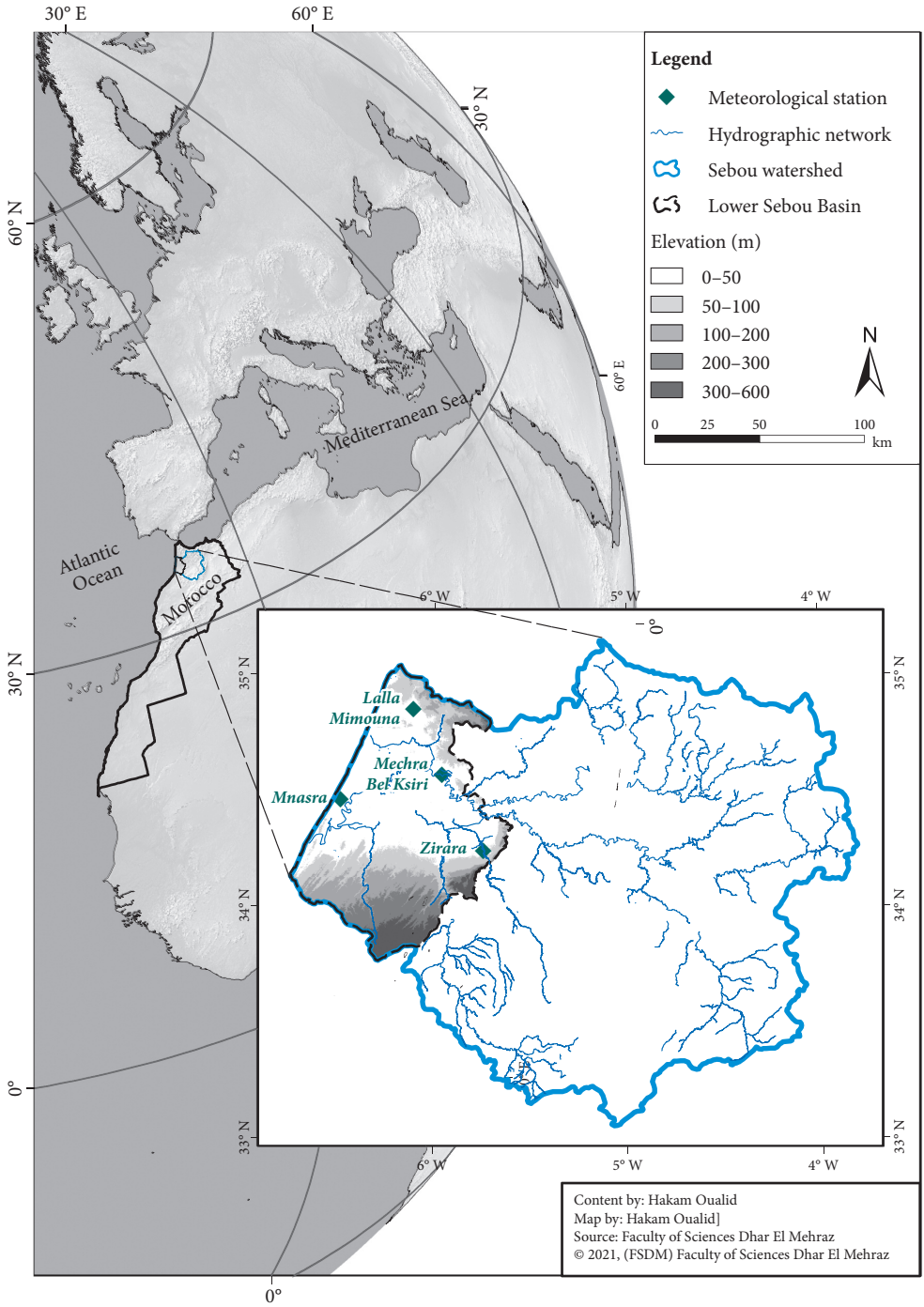

Figure 1: Geographical location of the LSB and location of the typical meteorological stations.

Figure 2: Main climatic teleconnections dominating in the LSB. ►

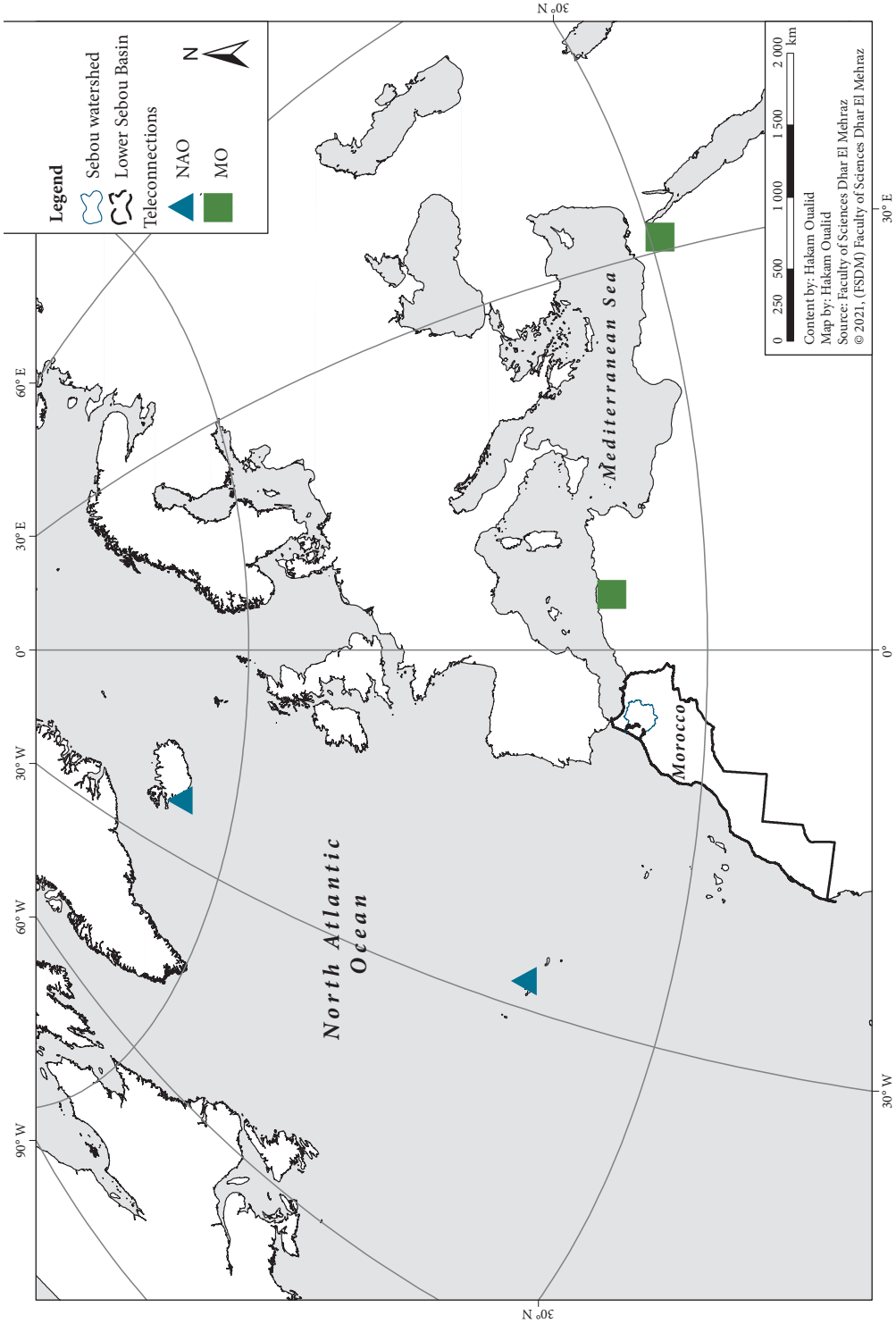
Legend
Sebou watershed
Lower Sebou Basin
Teleconnections
NAO
MO
N
30° N
60° E
30° E
0°
30° W
60° W
90° W
North Atlantic Ocean
Mediterranean Sea
Morocco
0 250 500 1 000 1 500 2 000 km
Content by: Hakam Oualid
Map by: Hakam Oualid
Source: Faculty of Sciences Dhar El Mehraz
© 2021, (FSDM) Faculty of Sciences Dhar El Mehraz

study has targeted the meteorological characteristics of the drought and its relationship with large-scale atmospheric dynamics, such a study in the LSB as a large agricultural plain would help to put into perspective the investments under the Morocco-Green Plan strategy (38.6 billion dirhams) and the threatened infrastructure (Ministry of Agriculture and Maritime Fisheries 2020). This strategy aims to develop a modern and efficient agriculture that meets the requirements of national and international markets (22% of Morocco's total exports, i.e. approximately 5.57 billion dollars) (Harbouze et al. 2019). This study also opens doors for the development of drought early warning systems in North Africa as the dissemination of this data will allow proactive decisions on water use and agricultural practices.

2 Data used and methodology

2.1 Study area

The Sebou watershed, downstream of which the LSB is located in the North West of Morocco and covers an area of 40,000 km^2. It flows from the Middle Atlas Mountain and ranges over a length of 500 km to its outlet in the Atlantic Ocean (Figures 1, 2). Indeed, the LSB takes benefits from a sub–humid Mediterranean climate with an oceanic influence, particularly in its western part. Rainfall exceeds 500 mm per year in most of the basin and average temperatures oscillate around 19 °C (Table 1). Consequently, the abundance of rainfall and the importance of the basin's water and biophysical resources expose the basin to overexploitation of resources and vulnerability to the effects of drought in the future.

2.2 Data used

Meteorological data provided by the Regional Office for Agricultural Development (ROAD) from the four weather stations cover the period from 1984 to 2016. The distribution and characteristics of these stations are presented in Figure 1 and Table 1.

Two important large-scale climate anomalies were selected to analyse the main drivers of drought in the LSB: NAO (North Atlantic Oscillation) and MO (Mediterranean Oscillation) (Zamrane, Mahé and Laftouhi 2021). The NAO is called a meridional dipole of atmospheric pressure with centres of action near the Azores (37 °N, -25 °E) and Iceland (65 °N, -18 °E) (Figure 2). The Mediterranean Oscillation (MO) is defined as a dipolar behaviour of the atmosphere between the East–West sub–basins of the Mediterranean. This index measuring the intensity of the dipole was defined as the normalized 500 hPa height anomalies between Alger (36.4 °N, 3.1 °E) and Cairo (30.1 °N, 31.4 °E) (Figure 2) (Conte, Giuffrida and Tedesco 1989). The monthly NAO and MO data were extracted from the National Oceanic and Atmospheric Administration (NOAA).

2.3 Drought indices (DIs)

Drought indices (DIs) help converting the indicator variables such as temperature and rainfall into a numerical value to represent the extent of the water deficit in a way that is easy to understand. DIs used in this study, namely the Standardized Precipitation Index and the Standardized Precipitation–Evapotranspiration Index mainly characterize meteorological drought (Table 2).

Table 1: Characteristics of the meteorological stations of the LSB.

Stations	rainfall (mm per year)	Average temperature (°C per year)	PET (mm per year)	Geographical coordinates		
				Long (°W)	Lat (°N)	Z (m)
Lalla Mimouna	574.7	17.15	1157.5	6.11	34.85	15
Mechra Bel Ksiri	515	19.35	1441.4	5.96	34.57	24
Mnasra	567	16.65	1239.5	6.48	34.46	10
Zirara	387	19.05	1480	5.74	34.24	55

Note. PET: potential evapotranspiration calculated based on the Thornthwaite equation; Long: longitude; Lat: latitude; Z: elevation in meter.

Table 2: Characteristics of drought indices (DIs).

Drought indices (DIs)	Name	Variables	Probability distribution	Reference
SPI	Standardized Precipitation Index	P	Gamma	McKee, Doesken and Kleist (1993)
SPEI	Standardized Precipitation–Evapotranspiration Index	P and PET	Log–Logistic (3 parameters)	Vicente-Serrano, Beguería and López-Moreno (2010)

Note. P: Monthly–accumulated precipitation; PET: Potential Evapotranspiration.

Standardized Precipitation Index (SPI) is based on historical rainfall records at a given location to calculate the probability of rainfall at any time-scale between 1 and 48 months.

$$SPI = \frac{Pi - Pm}{S} \tag{1}$$

With *Pi*: the rainfall of month or year *i*; *Pm*: the average rainfall of the month or year *i* in the entire period; *S:* the standard deviation of the series over the considered time-scale. Data were normalized using the gamma distribution method to overcome the constraint of rainfall that is not normally distributed over the year (Stagge et al. 2015).

Standardized Precipitation–Evapotranspiration Index (SPEI) is an index developed by Vicente-Serrano, Beguería and López-Moreno (2010). The procedure for calculating the SPEI is also similar to that of the SPI, except that it uses the difference between rainfall and potential evapotranspiration (PET) calculated according to the method of Thornthwaite (1984). In the SPEI calculation, we need the monthly water balance (D_i), which is based on the difference between rainfall and potential evapotranspiration (PET). This represents a simple climatic water balance calculated at different time-scales (1-, 3-, 6- and 12-months).

The difference between accumulated monthly rainfall and potential evapotranspiration was calculated as follows:

$$D_i = P_i - PET_i \tag{2}$$

Subsequently, the monthly D_i values are aggregated over different time-scales as is the case for rainfall in SPI calculations. A three–parameter Log–logistic distribution of D_i values was used to fit the data series of accumulated monthly difference values (Vicente-Serrano and Beguería 2016). Therefore, negative SPEI values indicate a dry condition due to lack of rainfall and/or higher PET compared to the historical average recorded.

The D_i values were summarized on different time-scales:

$$D_n^k = \sum_{i=0}^{k=1} (P_{n-i} - PET_{n-1}), n \geq k \tag{3}$$

where k is the monthly time-scale and n is the number of calculations. D_i values are aggregated depending on the time-scale before being standardized using the Log–logistic distribution with the following probability density function (Vicente-Serrano, Beguería and López-Moreno 2010; Pyarali et al. 2022):

$$\mathrm{f(x)} = \frac{\beta}{\alpha} \left(\frac{x-\gamma}{\alpha}\right)^{\beta-1} \left[1 + \left(\frac{x-\gamma}{\alpha}\right)^{\beta}\right]^{-2} \tag{4}$$

where α, β, and γ are scale, shape, and origin parameters, respectively. The probability distribution function of D_i according to the Log–logistic distribution is then given by:

$$\mathrm{F(x)} = \left[1 + \left(\frac{\alpha}{x-\gamma}\right)^{\beta}\right]^{-1} \tag{5}$$

The SPEI can easily be obtained as the standardized values of F(x). For example, following the classical approximation of Abramowitz and Stegun (1965):

$$SPEI = \omega - \frac{c_0+c_1\omega+c_2\omega^2}{1+d_1\omega+d_2\omega^2+d_3\omega^3} \quad (6)$$

Where

$$\omega = \sqrt{-2\ln(p)}$$
$$c_0 = 2.515517, c_1 = 0.802853, c_2 = 0.010328$$
$$d_1 = 1.432788, d_2 = 0.189269, d_3 = 0.001308 \quad (7)$$

p is the probability of exceeding a determined D_i value, p= 1–F(x). If $p > 0.5$, then p is replaced by $1 - p$ and the sign of the resultant SPEI is reversed. The category of SPI and SPEI varies from ≥ 2.0 (extremely wet) to ≤ -2.0 (extremely dry) (Table 3).

Table 3: Wet/Dry classification of SPI and SPEI. The colour scale indicates the drought classes in figure 6.

SPI/SPEI	Values	Class
	≥ 2	Extremely wet
	1.5 to 1.99	Very wet
	1 to 1.49	Moderately wet
	–0.99 to 0.99	Near normal
	–1 to –1.49	Moderately dry
	–1.5 to –1.99	Severely dry
	≤ –2	Extremely dry

2.4 Identification and characterization of drought events

The »runs« theory proposed by Yevjevich (1967) has been applied to identify and characterize meteorological drought events based on DIs. A drought event is defined as a consecutive sequence of months (t) with a drought index value (Xt) below a chosen threshold (X0); hence each drought event is characterized by the following parameters (Figure 3):

- drought duration (D) is defined as the time interval between the beginning and the end of a drought event;
- drought intensity (Is) is defined as the number of months during which the DIs values are lower than –1;
- drought severity (S) is defined as the sum of the monthly DIs values when they are lower than –1 (X0) during the period considered;
- peak intensity indicates the lowest DIs value during a drought event.

2.5 Trend analysis (Mann–Kendall test)

The Mann Kendall (M–K) trend test helps to find the presence of a monotonic trend in a time series of hydro–climatic variables (Acharki et al. 2019). In the case of the LSB, the M–K test is applied to analyse the temporal characteristics of the SPI and SPEI indices.

The test is based on the (*S*) statistic defined as follows:

$$S = \sum_{k=1}^{N-1}\sum_{j=k+1}^{N} sng(x_j - x_k) \quad (8)$$

Where S is the number of positive differences minus the number of negative differences, N is the number of data points, x_j and x_k are monthly values of months j and k with $(j > k)$.

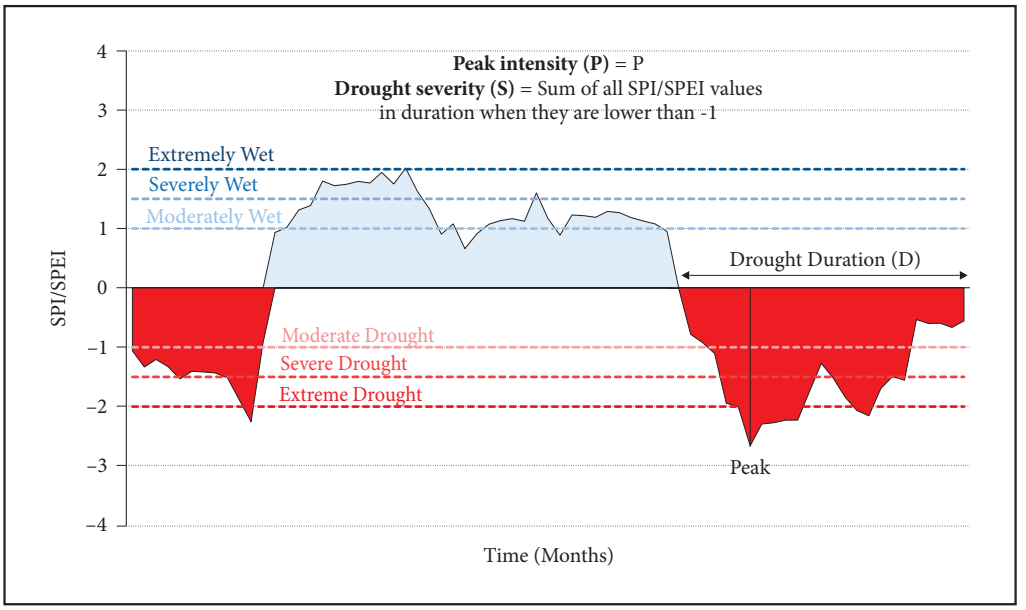

Figure 3: Drought characteristics for DIs following the »Run« theory.

Noting $\varepsilon = (x_j - x_k)$

$$sng(\varepsilon) = \begin{cases} 1 \; if \; \varepsilon > 0 \\ 0 \; if \; \varepsilon = 0 \\ -1 \; if \; \varepsilon < 0 \end{cases} \tag{9}$$

When $N > 10$, the distribution of S is assumed to be normally distributed with mean $E(S) = 0$ and variance ($var(S)$) given by:

$$var\,(S) = \frac{N(N-1)(2N+5) - \sum_{k=1}^{n} t_k(t_k-1)(2t_k+5)}{18} \tag{10}$$

where N is the number of tied (zero difference between compared values) groups and t_k the number of data points in the k^{th} tied group. Then the values of S and $var(S)$ are used to calculate the standardized statistical test Z under the following formula:

$$Z = \begin{cases} \frac{S-1}{\sqrt{var(S)}} & if \; S>0 \\ 0 & if \; S=0 \\ \frac{S+1}{\sqrt{var(S)}} & if \; S<0 \end{cases} \tag{11}$$

A positive (negative) value of Z indicates an ascending (descending) trend and its significance is compared to the critical value α or significance level of the test. Absolute values of $Z \geq 1.65$, 1.96 and 2.58 are adopted, respectively, indicating significant levels of (α) 0.1, 0.05 and 0.01.

In order to find a monotonic trend in the time series used, it is necessary to identify the period of the beginning of the trends. Therefore, the Sequential Mann–Kendall (SQMK) test statistic is particularly useful for such change detection analysis (Gerstengarbe and Werner 1999). The SQMK test procedure is different from the Z test and consists of the following steps:

- Values of the series x are replaced by their ranks r_i, ranked in ascending order;
- Quantities r_i ($i = 1, 2, \ldots, n$) are compared with r_j ($j = 1, 2, \ldots, i - 1$);

- Statistic t_i is defined as follows:

$$t_i = \sum_{k=1}^{i} n_k \tag{12}$$

- Variance of the statistic var (t_i) and the mean E (t_i) of the test is calculated as follows:

$$E(t_i) = \frac{i(i-1)}{4} \tag{13}$$

and

$$var(t_i) = \frac{i(i-1)(2i+5)}{72} \tag{14}$$

- Values of $u(t_i)$ statistic can then be calculated as:

$$u(t_i) = \frac{[t_i - E(t_i)]}{\sqrt{var(t_i)}} \tag{15}$$

While the forward sequential statistic, $u(t_i)$ is estimated using the original time series $x_1, x_2 \ldots x_n$, values of the backward sequential statistic, $u'(t_i)$ are estimated in the same manner but starting from end of the series. In estimating $u'(t_i)$ the time series is resorted so that last value of the original time series comes first $x_n, x_{n-1} \ldots 1$. The sequential version of Mann–Kendall test statistic allows detection of approximate beginning of a developing trend. When $u(t_i)$ and $u'(t_i)$ curves are plotted, the intersection of the curves $u(t_i)$ and $u'(t_i)$ locates approximate potential trend turning point. If the intersection of $u(t_i)$ and $u'(t_i)$ occur within ± 1.96 (95% confidence level) of the standardized statistic Z, a detectable change at that point in the time series can be inferred. Moreover, if at least one value of the reduced variable is greater than a chosen level of significance of Gaussian distribution the null hypothesis (H_0: Sample under investigation shows no beginning of a new trend) is rejected.

2.6 Drought events and large-scale climate anomalies

To search for possible relationships, wavelet coherence analysis was applied to DIs (SPI and SPEI) and large-scale climate anomaly indices, such as NAO and MO. Wavelet coherence is an approach used for analysing the degree of coherence of cross wavelet transform in time-frequency space. It has been widely used to analyse the periodicity of drought and the relationships between hydrological variability and possible teleconnections (Zamrane, Mahé and Laftouhi 2021).

Following Torrence and Webster (1999), the wavelet coherence coefficient can be defined as follows (Chang et al. 2019):

$$R^2(\alpha,\tau) = \frac{|S(\alpha^{-1}W_{xv}(\alpha,\tau))|^2}{S(\alpha^{-1}|W_x(\alpha,\tau)|^2) * S(\alpha^{-1}|W_y(\alpha,\tau)|^2)} \tag{16}$$

where $R^2(\alpha, \tau)$ takes values between 0 (no coherency) and 1 (perfect coherency), α is the scale expansion parameter, τ is the dimensionless time–shift parameter, $W_{xy}(\alpha, \tau)$ is the cross wavelet transform of the two time series, W_x and W_y are the sums of ranks of observations in samples x_t and y_t, respectively, and S represents a smoothing operator, which is defined as:

$$S(W) = S_{scale}(S_{time}(W(\alpha,\tau))) \tag{17}$$

where S_{scale} and S_{time} represent smoothing along the wavelet scale axis and in time, respectively.

3 Results

3.1 Temporal evolution of the SPI and SPEI

The monthly SPI and SPEI values that have been calculated on four time scales (1-, 3-, 6- and 12-months) can be used for the monitoring and evaluation of different types of droughts and their full application can allow a comprehensive detection and evaluation of droughts and floods. They were first calculated using the two monthly climate data observed from four weather stations over the period from 1984 to 2016 (Figure 4). Then, the time series of SPI and SPEI were averaged over the four stations to characterize the dry or wet conditions in the LSB. Figure 4 shows the process of SPI and SPEI changes at different time-scales (1-, 3-, 6- and 12-months) during the period 1984–2016. Both indices indicated an extreme severity of drought after the beginning of the 21st century where the frequency and intensity of drought periods are increased. Noting that longer the time-scale, the more obvious the severity and duration of the drought. Typical drought periods or years occurred in 1992–1995, 1999–2002, 2005–2006, 2012 and 2015–2016 by applying SPI–12 and SPEI–12. However, the indices fluctuated frequently, with a wide range, on time scales of 1- and 3-months, which suggests the impact of short–term climate change. In addition, the range of positive and negative fluctuations of SPI was larger than that of SPEI. However, on longer time-scales (6- and 12-months), SPI and SPEI values had a smooth trend, the volatility has decreased and the characteristics of inter-annual and inter-decadal changes were evident, hence the duration of the drought increased. The temporal trend of SPI and SPEI showed a relatively stable evolution and a smaller amplitude difference at different time-scales, but there are slight differences in the fluctuation value and continuity, explaining different drought intensities and frequencies. The difference between SPI and SPEI decreased with the increase of the time-scale, where the values fluctuated between -4 and 4 at short time-scales (1-month) and between –1 and 1 at long time-scales (12-months). Furthermore, it should also be noted that this difference has increased in recent years (Figure 5).

3.2 Monthly variations of the SPI and the SPEI

The SPI and SPEI monthly distribution values were quite clear at different time-scales, which can reflect the variation of dry and wet conditions for each month in the LSB (Figure 6). It was clear that the duration and intensity of drought in some months has increased considerably and the effect of time-scales on drought duration and intensity was evident, particularly after the beginning of the 21st century. It is also observed that the droughts reflected by SPI and SPEI were slightly different in each month and at different time-scales, especially on the 1– and 3-months scales. Thus Figure 6 shows that the distribution of drought expressed by the SPI was random on short scales (1-month and 3-months), especially in the winter season. The dry months reflected by SPEI–1 and SPEI–3 were concentrated in the winter months before 2004, and after this year the dry months start to shift towards the summer and into the end of the year (December). Furthermore, droughts reflected by SPEI were more frequent on short time-scales, especially 1-month, while droughts reflected by SPI were common on 6-months and 12-months scales; which reflects the effect of the evapotranspiration parameter included in the SPEI calculation on the variation in drought conditions in the LSB.

3.3 Temporal variability

The evolution of SPEI and SPI values and the annual and seasonal trends, as well as the graphical results of the SQMK test identified the year when the turning point and the magnitude of the change occurred in the LSB. Knowing that the identified turning point and the magnitude of change year for each period represent the beginning of a negative or positive trend (Figure 7).

Figure 4: Temporal evolution of SPI and SPEI at time-scales of 1-, 3-, 6- and 12-months in the LSB during 1984–2016. ► p. 34
Figure 5: Difference (D) between the SPI and SPEI indices in the different time-scales (1-, 3-, 6- and 12-months) in LSB during 1984–2016. ► p. 35
Figure 6: Heat monthly variation in the SPI and SPEI at 1-, 3-, 6- and 12-months' time-scales during 1984–2016 in the LSB, colour legend indications are obtained in Table 3. ► p. 36

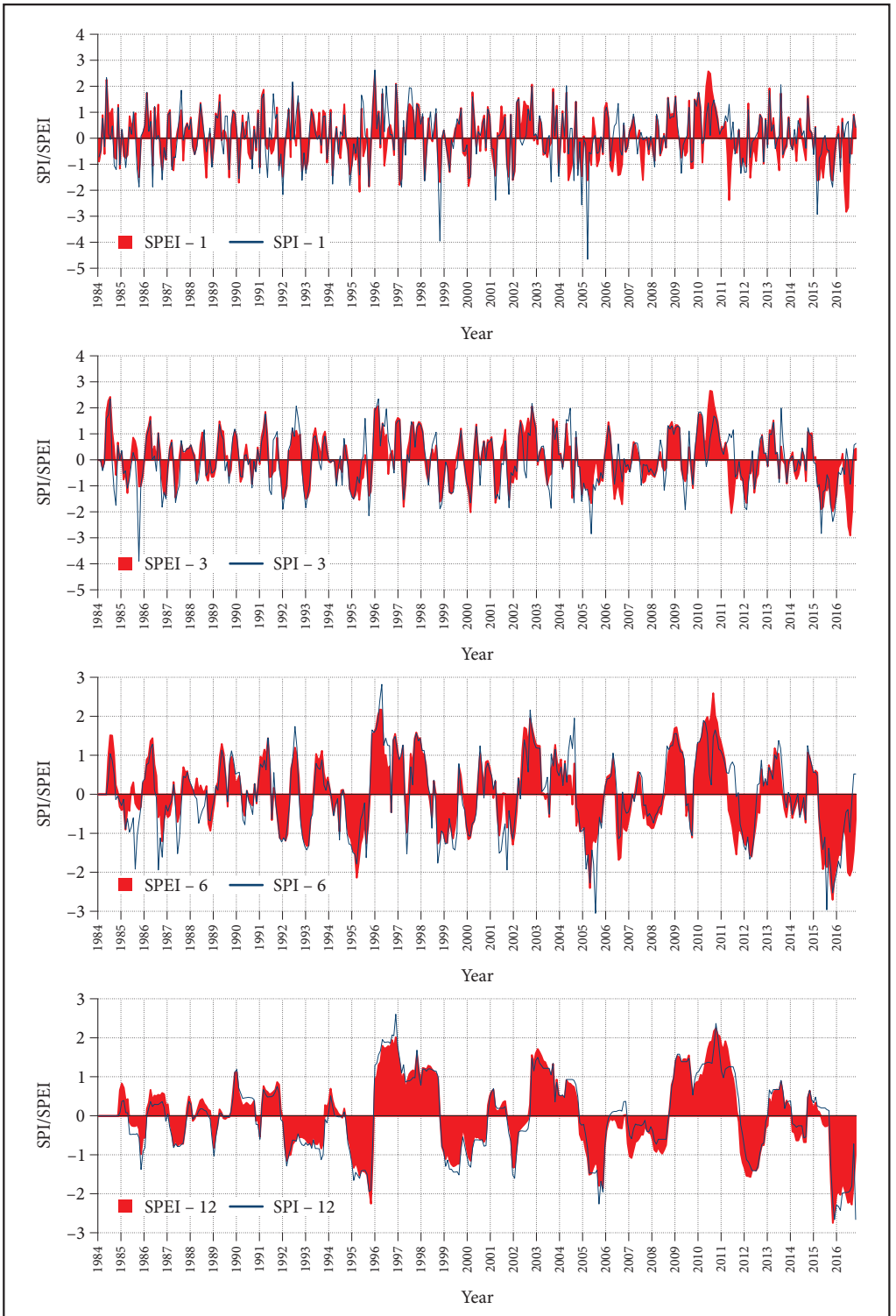
SPI/SPEI
SPEI – 1
SPI – 1
Year
SPI/SPEI
SPEI – 3
SPI – 3
Year
SPI/SPEI
SPEI – 6
SPI – 6
Year
SPI/SPEI
SPEI – 12
SPI – 12
Year

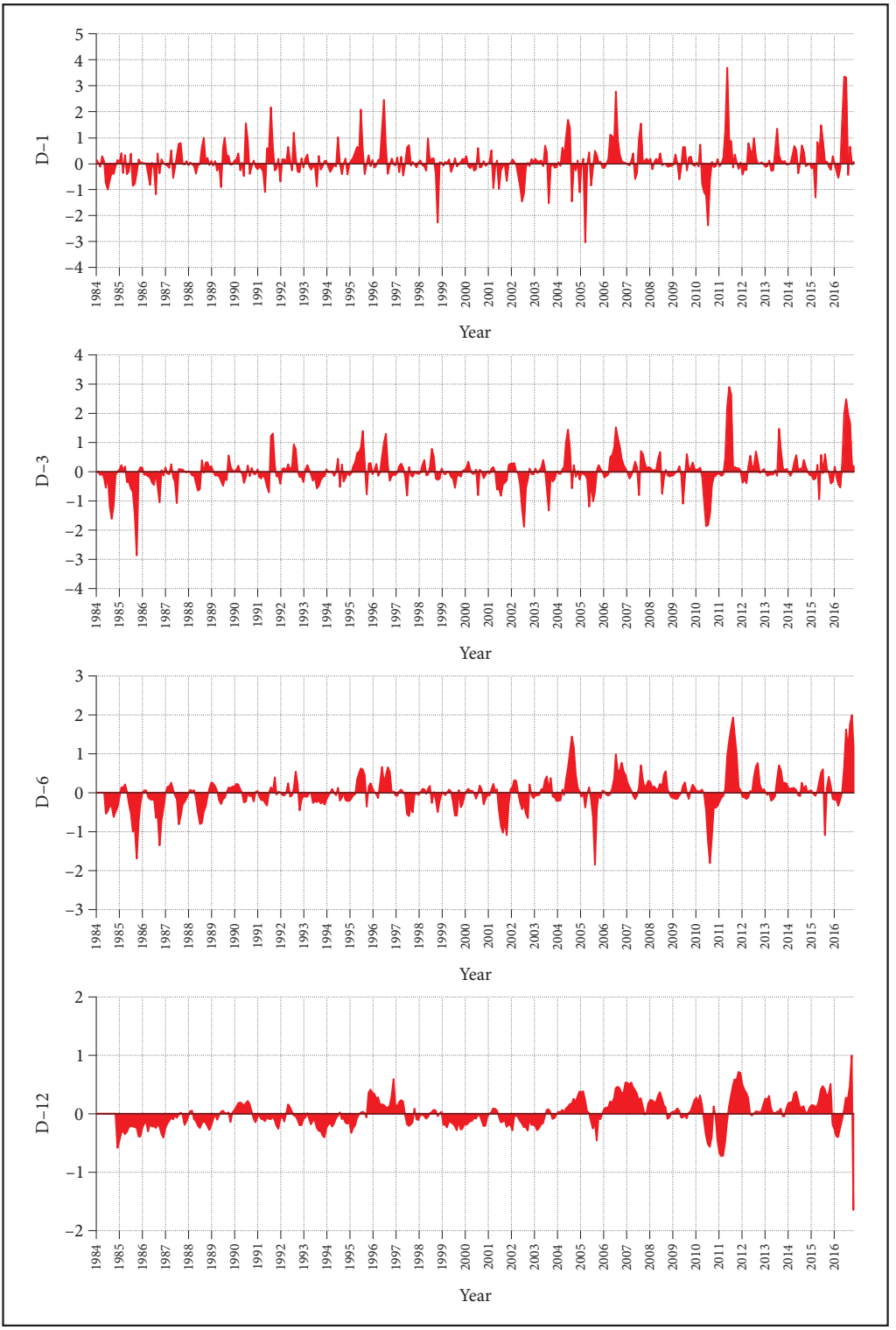
D–1
D–3
D–6
D–12
Year

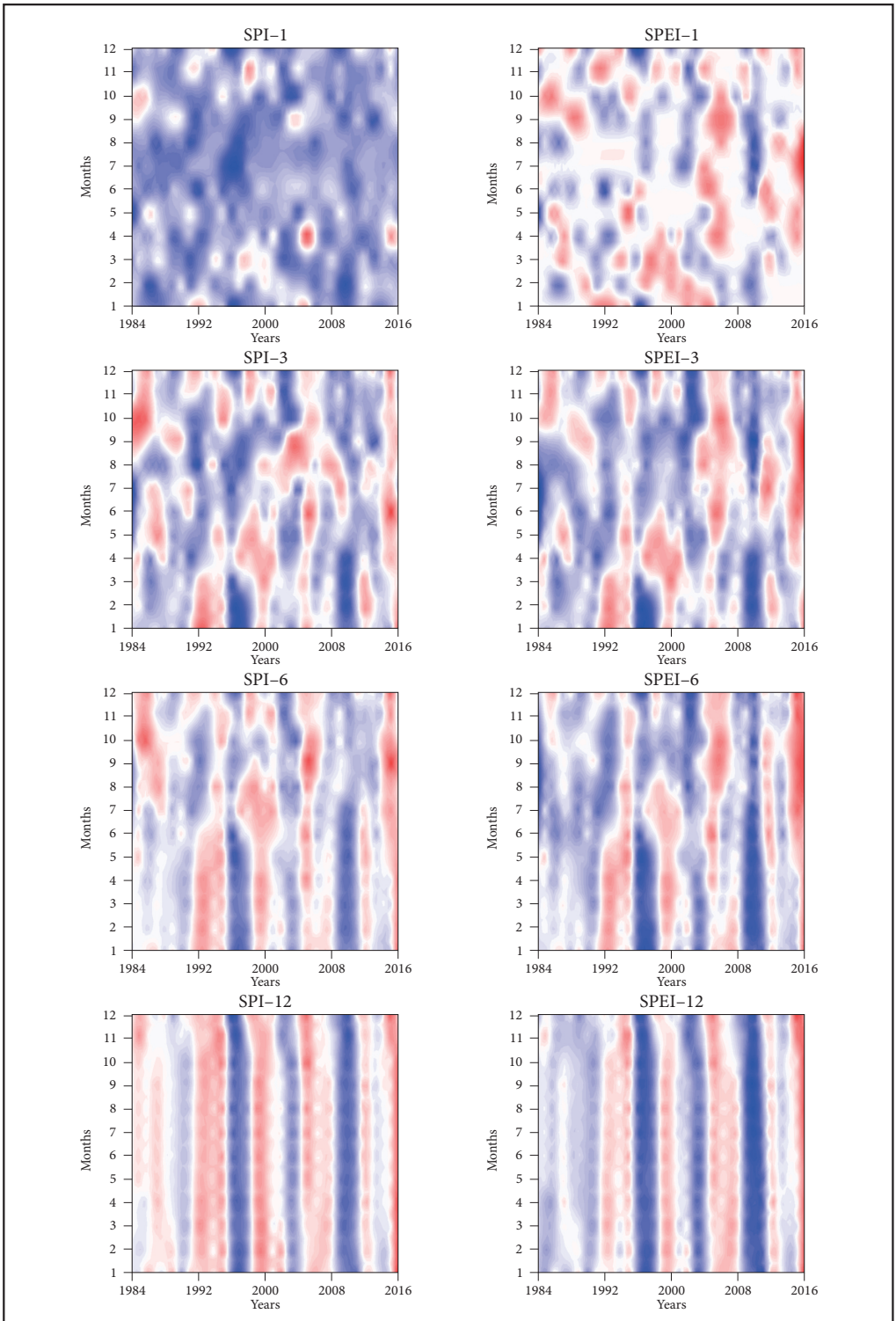
SPI–1
SPEI–1
SPI–3
SPEI–3
SPI–6
SPEI–6
SPI–12
SPEI–12
Months
Years
1
2
3
4
5
6
7
8
9
10
11
12
1984
1992
2000
2008
2016

The annual and seasonal (winter, spring, summer and autumn) Z_{SPEI} values were –0.85, –0.50, –0.26, –3.51 and 0.54 respectively, and showed a decreasing trend, except for the autumn season (Z_{SPEI} = 0.54). While the annual and seasonal Z_{SPI} values were 0.39, –0.60, –0.23, –2.25 and 1.07 respectively, in contrast to SPEI, Z_{SPI-12} showed an increasing trend (Figure 7). According to the SPI and SPEI drought indices, extreme drought events on an annual scale were observed in 2006 and 2016 (Figures 7). For seasonal droughts, winter was the most affected by drought followed by spring, however the SPEI considered autumn as the least drought–prone season. It is worth noting that u(t) and u'(t) curves of SPI at the annual and autumn scales were in very good agreement with each other, which might suggest that annual rainfall is mainly impacted by autumn rainfall (Figure 7). In general, the SPI and SPEI series showed high variability, with no significant trends over the study period, except for the summer when the most severe droughts were recorded only from the year 2000 onwards. As shown in Figure 7, the downward trends in summer were highly significant from 2004 to 2016 at 95% significance level, hence the intersection of the u(t) and u'(t) curves of SPI–3 and SPEI–3 during the summer season occurred in 1998 and 2003, respectively, and exceeded the confidence limit in 2004 (Fig. 7). This is clearly indicated in the monthly variation of SPEI–3 and SPI–3 in Figure 6.

3.4 Spatial and inter-annual variability

At the annual scale, the spatial distribution of the drought duration trends of SPI and SPEI was interpolated by the Inverse Distance Weight interpolation method (IDW method) (Figure 8a). The drought duration reflected by SPI–12 and SPEI–12 was identical with an opposite spatial distribution. In terms of trends, all stations showed non–significant increasing trends; however, the SPI–12 suggested that the two stations (Lalla Mimouna and Mnasra) showed a decreasing trend (tendency to be wet). Whereas, the other stations showed an increasing trend, mainly located in the interior of LSB. The duration of droughts in the LSB increased from West to East. The SPEI–12 showed that the duration of drought is longer in the western regions and shorter in the north-eastern part of the basin.

The spatial distribution of drought severity trends in the LSB was different from that of drought duration, where the Mnasra station recorded the longest period and the least severe at the same time (Figure 8b). However, the SPI–12 and SPEI–12 indices showed a similar overall behaviour of the drought severity distribution except for the Zirara station. Droughts were more frequent in the Northeast of the basin, especially in the Mechra Bel Ksiri station. In terms of trend, all stations showed increasing trends, only Lalla Mimouna and Mechra Bel Ksiri stations recorded a significant increasing trend for SPEI and SPI respectively, mainly in the North West and Northeast of the LSB. In general, droughts occur within the basin showing significant upward trends.

3.5 Correlations between SPI and SPEI

Pearson correlation plots between SPI and SPEI series were made at different time-scales for each station (Figure 9). The relationships between this DIs at different time-scales had relatively high correlation coefficients (r). However, there was a marked difference in the correlation coefficient (r) of each station at different time-scales, especially at the 1-month time-scale. On the short time-scales (1- and 3-months), the correlation coefficients (r) between SPI and SPEI were relatively low in the summer period ($r < 0.5$). As the time-scale increased, the low correlation coefficients shifted towards the autumn season on a 6-months' time-scale. On an annual scale of 12-months, in all stations there were very strong correlations ($0.7 < r < 0.95$) except the Zirara station ($0.4 < r < 0.6$). The correlation between SPI and SPEI in the western part of the LSB was generally higher than in the eastern part (Zirara station) since SPI neglected the temperature variation in the calculation and PET is high at this station (Table 1).

Therefore, the droughts identified by SPI and SPEI may be different in the East of the LSB (Figure 9).

Figure 7: Seasonal and annual variations of M–K trend test and abrupt changes in SPEI (left) and SPI (right) in the LSB during 1984–2016. ➤ p. 38–39
Figure 8: Distribution of trends in drought duration (a) and drought severity (b) for SPEI (left) and SPI (right). Significant positive trend ($Z > 1.96$), insignificant trend ($-1.95 < Z > 1.96$) and significant negative trend ($Z < -1.95$). ➤ p. 40
Figure 9: The correlations between the SPI and SPEI of typical meteorological stations in the LSB at scales of 1-, 3-, 6- and 12-months. Correlations significant at the 95% confidence level are indicated by triangles. ➤ p. 41

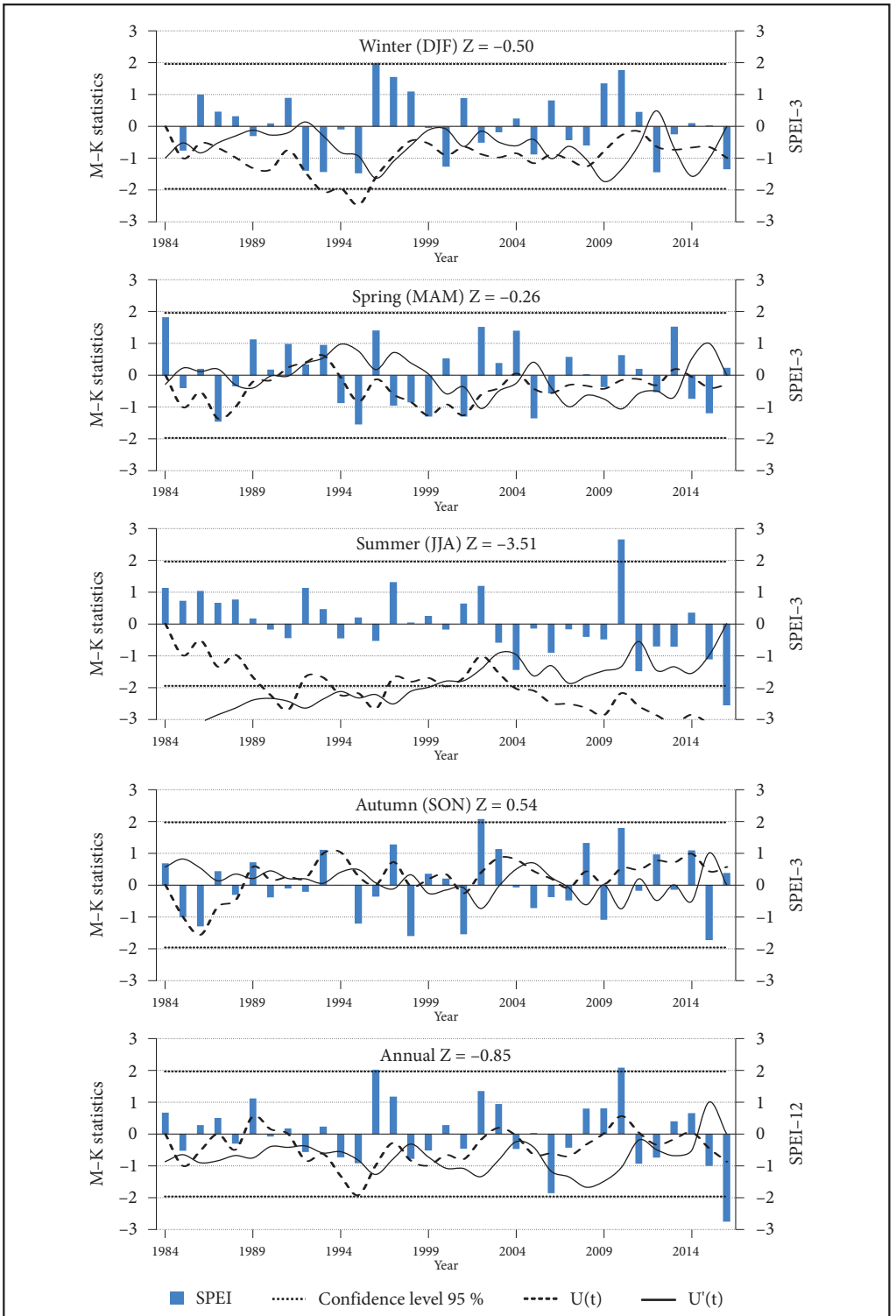
Winter (DJF) Z = –0.50
Spring (MAM) Z = –0.26
Summer (JJA) Z = –3.51
Autumn (SON) Z = 0.54
Annual Z = –0.85
M–K statistics
SPEI–3
SPEI–12
Year
1984
1989
1994
1999
2004
2009
2014
SPEI
Confidence level 95 %
U(t)
U'(t)

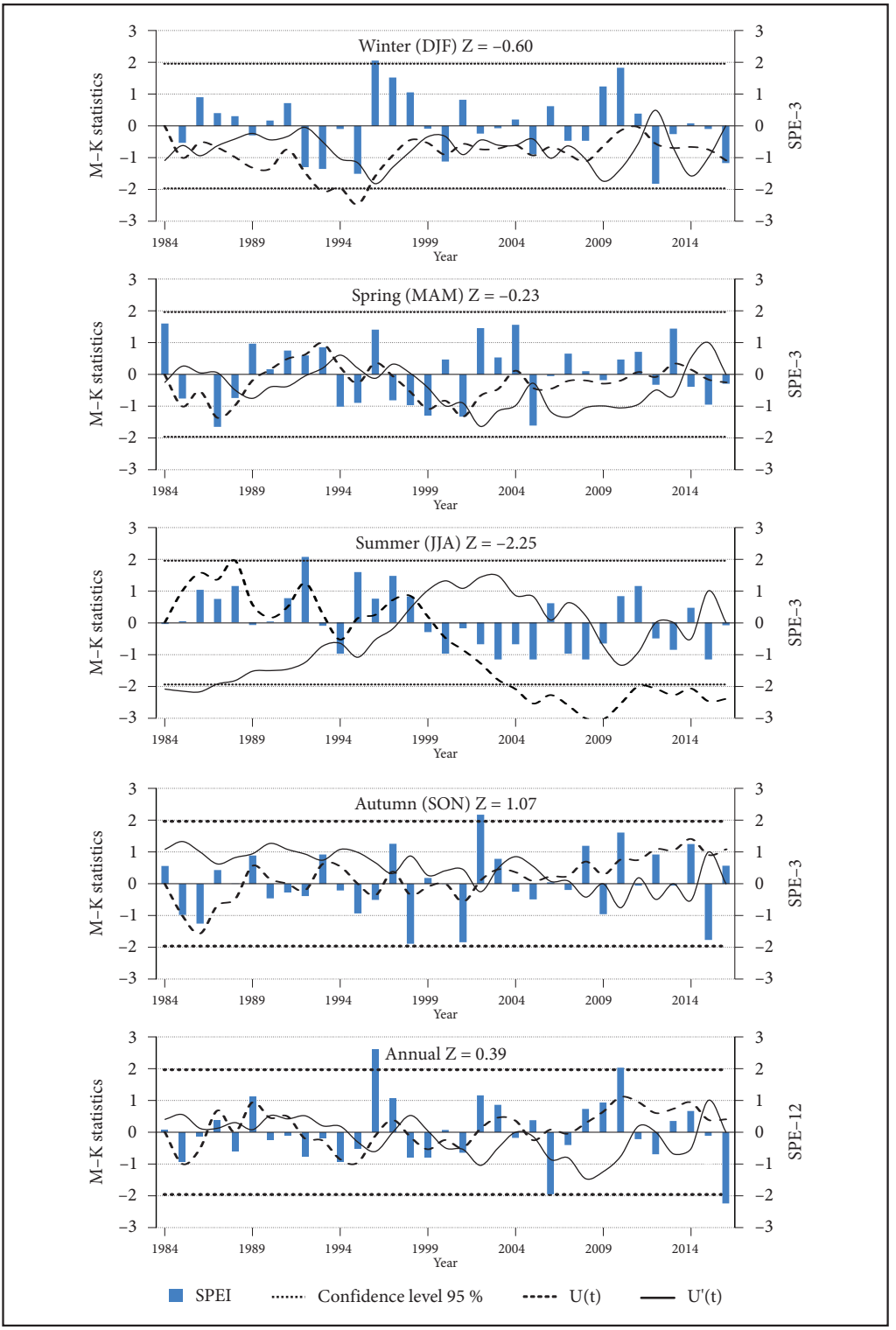
Winter (DJF) Z = –0.60
Spring (MAM) Z = –0.23
Summer (JJA) Z = –2.25
Autumn (SON) Z = 1.07
Annual Z = 0.39
M–K statistics
SPE–3
SPE–12
Year
1984
1989
1994
1999
2004
2009
2014
SPEI
Confidence level 95 %
U(t)
U'(t)

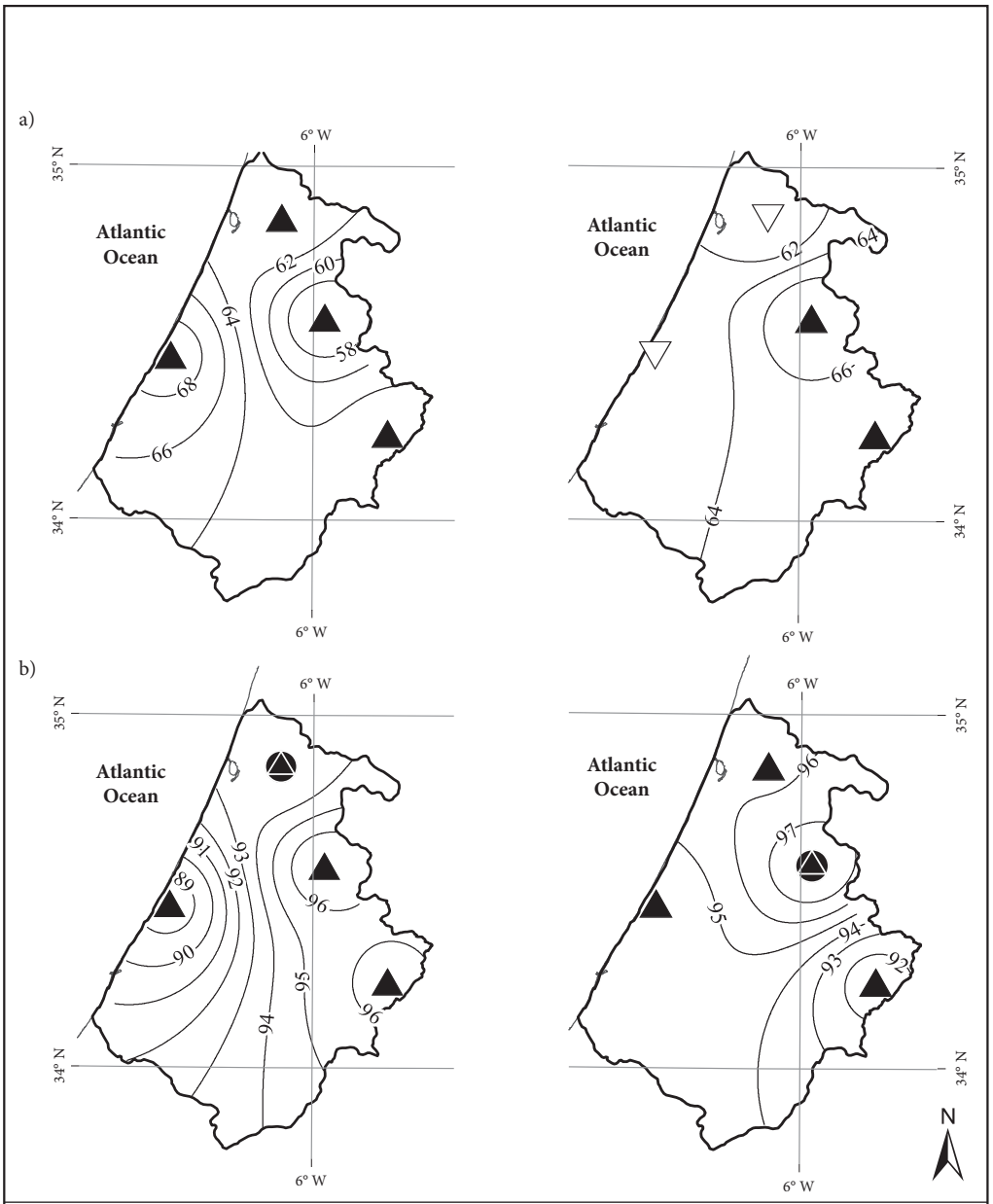
a)
b)
6° W
35° N
34° N
Atlantic Ocean
62
60
64
58
68
66
64
62
64
66
64
91
89
92
90
96
95
94
96
96
97
95
94
93
92
N
Legend
Z value
−2.96 to −1.96
−1.96 to 0
0.01 to 1.95
1.96 to 2.96
0 10 20 40
km
Content by: Hakam Oualid
Map by: Hakam Oualid
Source: Faculty of Sciences Dhar El Mehraz
© 2021, (FSDM) Faculty of Sciences Dhar El Mehraz

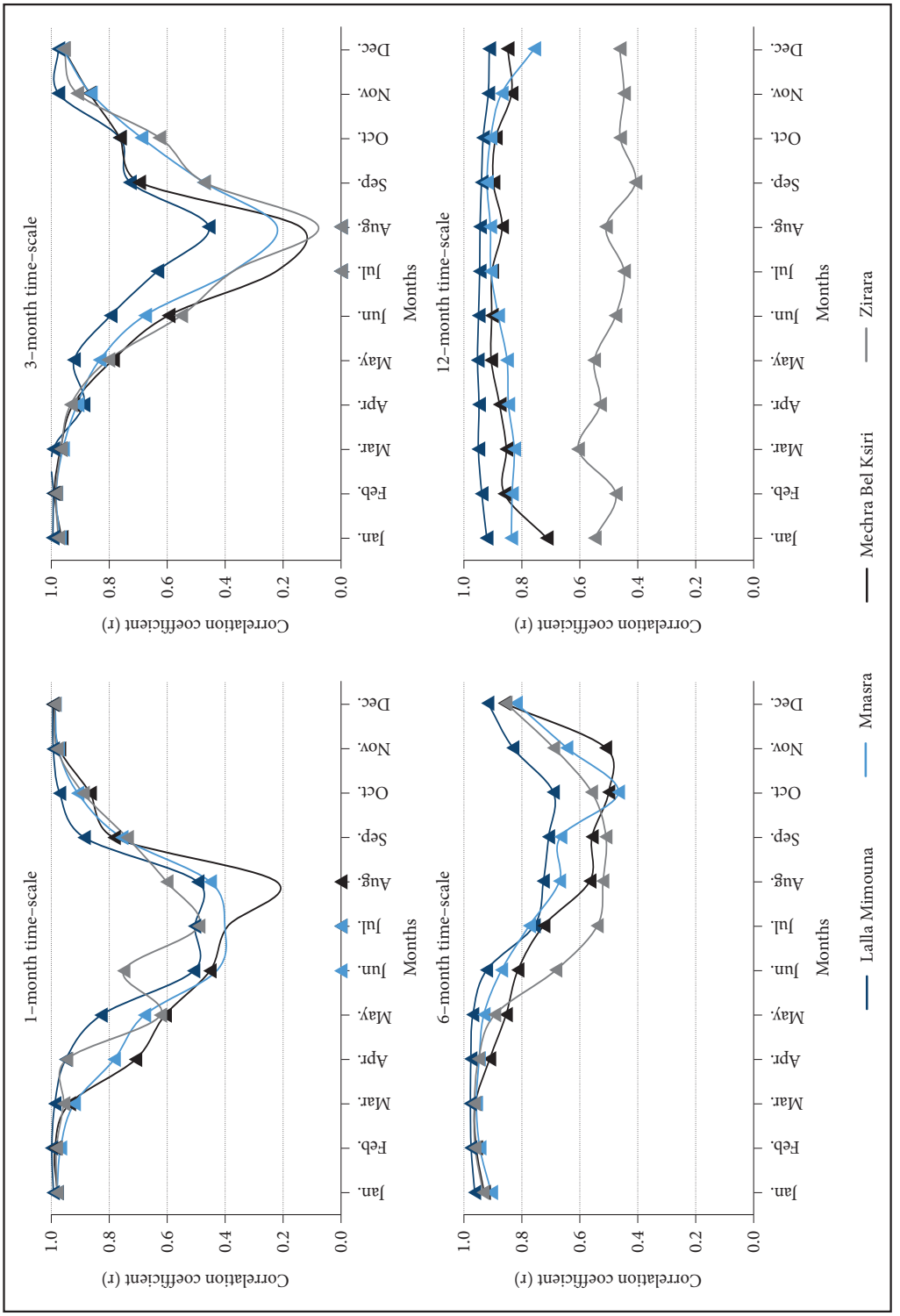
1–month time–scale
3–month time–scale
6–month time–scale
12–month time–scale
Correlation coefficient (r)
1.0
0.8
0.6
0.4
0.2
0.0
Jan.
Feb.
Mar.
Apr.
May.
Jun.
Jul.
Aug.
Sep.
Oct.
Nov.
Dec.
Months
Lalla Mimouna
Mnasra
Mechra Bel Ksiri
Zirara

3.6 Coherence between drought indices (DIs) and large-scale climate indices

Wavelet coherence (WC) identifies both the frequency bands and time intervals of co–variations between SPI/SPEI and large-scale climate indices (i.e. NAO and MO) in the LSB (Figures 10, 11). The WC, which varies in value from 0 to 1, measures the cross–correlation between the drought and climate indices as

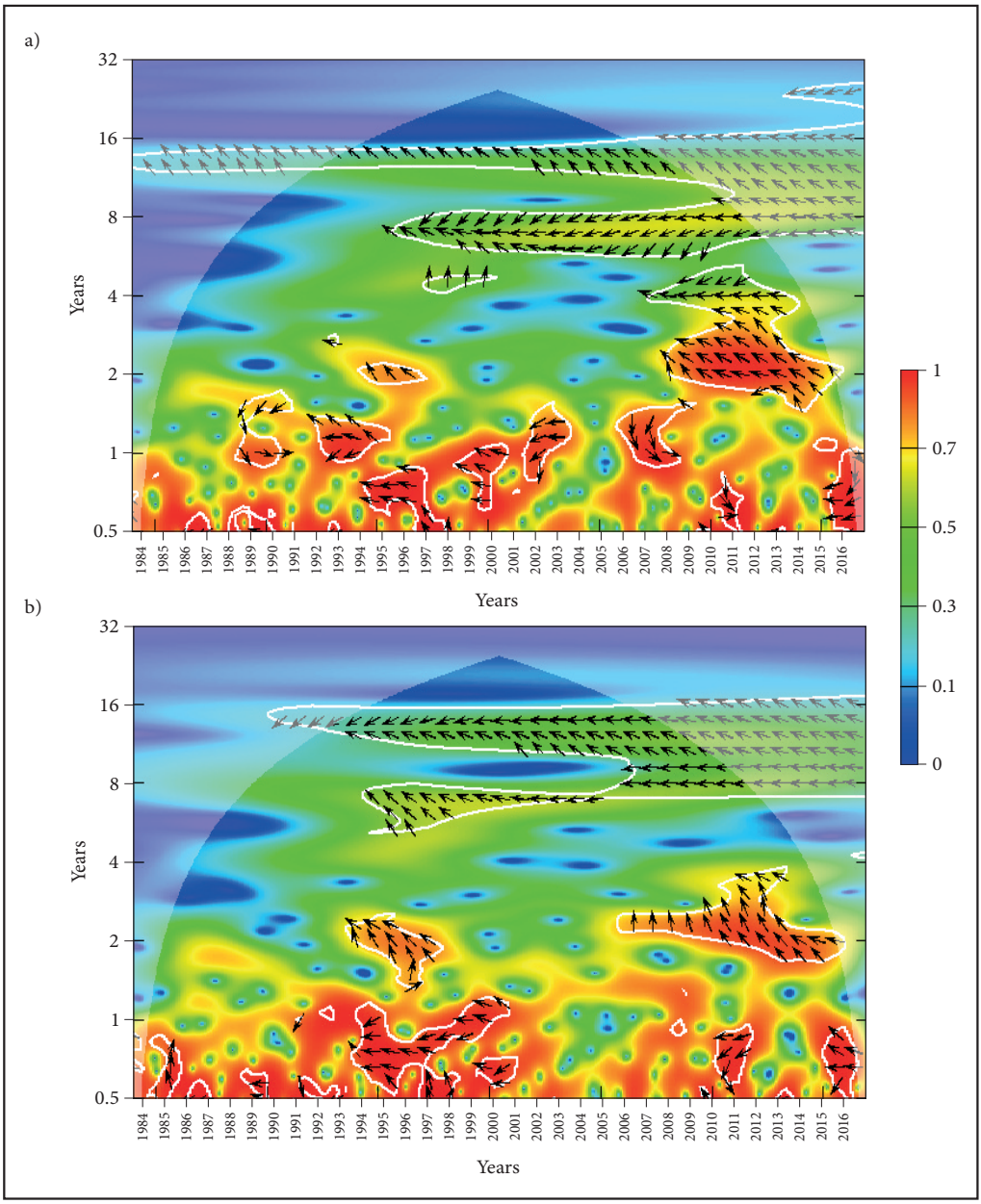

Figure 10: Wavelet coherence spectrum between the large-scale climate indices (NAO) and the SPEI (a) and SPI (b) series of the LSB. The colours from blue to red indicate increasing coherence. The 95% significance level with respect to the red noise is represented by a white outline.

a function of frequency. The coloured shading represents the magnitude of the coherence, as indicated in the colour bar, indicating the time-scale variability in the correlation between the two-time series. The white contours represent the significant sections that have a significance level of 95%. Arrows represent consistency (right–oriented: positive correlation, left–oriented: negative correlation). As shown in Figures 10 and 11, for a shorter periodicity of less than one year, significant coherence between the DIs (SPI and

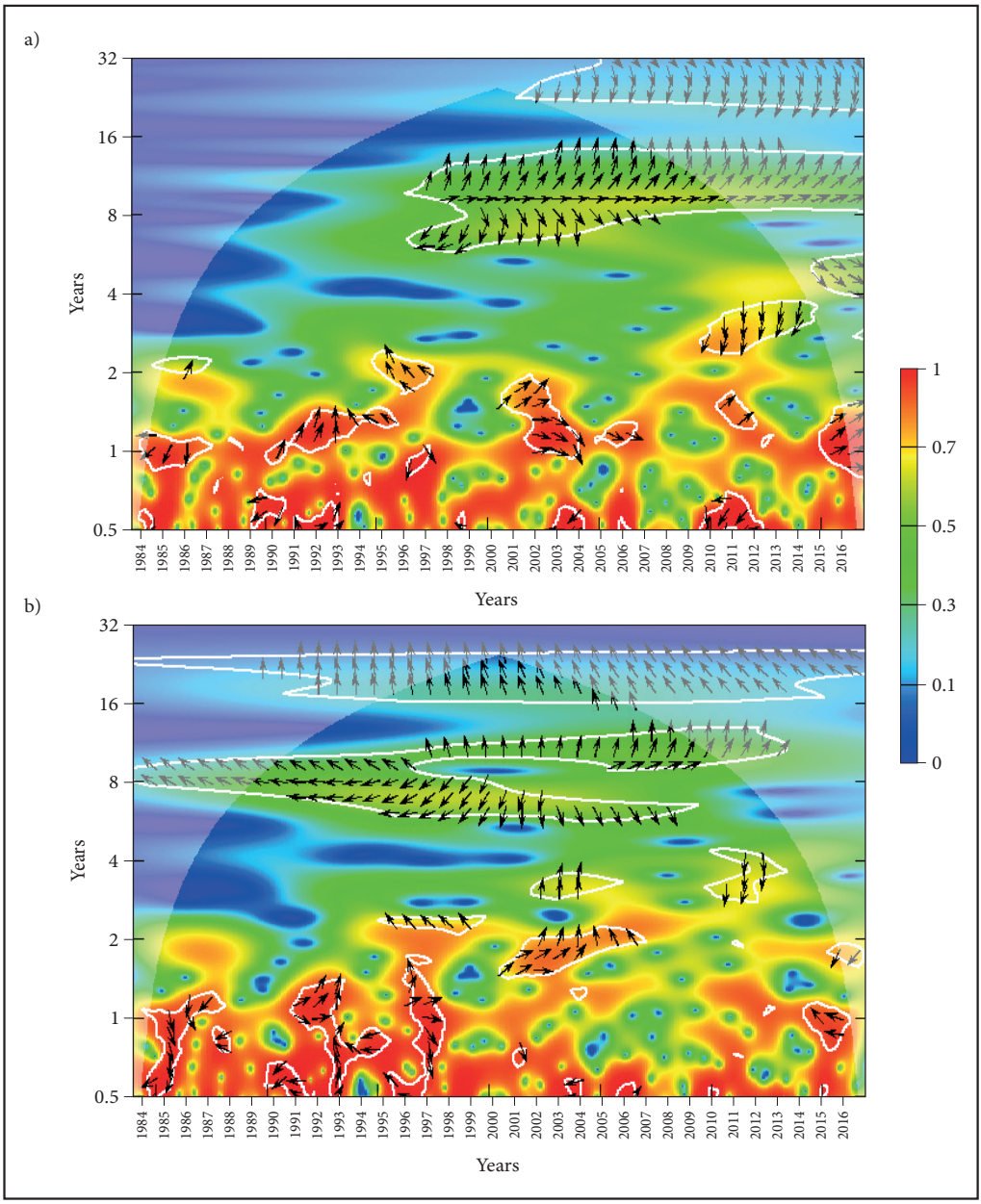

Figure 11: Wavelet coherence spectrum between the large-scale climate indices (MO) and the SPEI (a) and SPI (b) series of the LSB. The colours from blue to red indicate increasing coherence. The 95% significance level with respect to the red noise is represented by a white outline.

SPEI) and the climate indices (NAO and MO) was observed intermittently from year to year. Strong negative consistency is detected around 8–16 years (multi–annual) throughout the period considered (1984–2016). The NAO had the first–order relationship with drought variation over an 8–16 years' period, appearing since 1990 for SPI and during the whole period considered (1984–2016) for SPEI. Considerable energy is observed during a short period in the mid–1990s and from 2006 to 2015 for the 2–4 years' group (Figure 10). In the case of the MO, the coherence with the DIs (SPI and SPEI) was almost similar to that of the NAO but with low energy. The same energies are detected during the same periods of NAO (Figure 11). NAO has mostly strong negative coherence, while in MO the coherence is partly positive and partly negative.

4 Discussion and conclusion

The results reveal some differences between DIs in drought monitoring, found in most studies (Liu et al. 2021; Hakam et al. 2022a), which are due to the variation in climatic conditions at the different LSB stations and especially at the Zirara station (Figure 9). The fact that the calculation of DIs is based on rainfall and that the variability of rainfall is much higher than that of PET, considered stationary (without temporal trend), the importance of the latter would be negligible and drought conditions are almost controlled by the temporal variability of rainfall. However, some authors have cautioned against systematically neglecting the importance of the effect of temperature on drought conditions, and numerous empirical studies have shown that increasing temperature significantly affects drought severity (McGuire et al. 2010; Linares and Camarero 2012). Due to the consideration of temperature by SPEI, the evolution of annual drought showed a decreasing trend, while the drought reflected by SPI–12 showed an increasing trend, so the performance of SPI might be insufficient in reinforcing the conclusions on the warming trend of the climate in Morocco (Figure 7).

At the seasonal scale, both SPI–3 and SPEI–3 showed decreasing trends, except for autumn where SPI–3 recorded a positive value (Z_{SPI-3} = 1.07). This indicates that the fall season would be marked by a slight increase in rainfall and a shift in the wettest season of the year, as rainfall is relatively more abundant in the fall and less abundant in the winter (Z_{SPI-3} = –0.60). Consequently, the autumn drought that started in September was increasingly less severe in the LSB and when rains started early with high intensity, a winter drought would be expected (Figure 6). These results further confirm the findings of Acharki et al. (2019) and Diani et al. (2019). In addition, SPI–3 and SPEI–3 showed that the summer season was the most drought–prone with a significant downward trend at the 0.05 level, triggered in 2004 (Figures 6, 7). This triggering of dry months can explain the increase in average temperatures from the year 2004 (Driouech 2010). Thus, the intensification of drought episodes in summer was also related to the nature of the winds that prevail in this season, namely the warm continental winds from the southeast (Chergui and Sirocco). These winds led to high evapotranspiration marked by the trend of SPEI–3 to the lowest value of Z (Z_{SPEI-3} = –3.52) and the small amounts of rainfall received are mainly of stormy origin (Z_{SPEI-3} = –2.25). Concerning the winter season, no month escaped the drought either by SPI–3 or by SPEI–3 and even on different time-scales. The abnormal dryness of the rainy season months was due to a relative frequency of random anticyclonic situations. This winter drought seemed to change from month to month, and was shorter than in the summer season (Figure 6). The reason for this is that winter anticyclonic situations, generating dry and cold weather, are less persistent than stable and hot summer weather (summer anticyclones), therefore more quickly degraded by rainfall disturbances.

The climate in LSB is subject to the contrasts of the Mediterranean climate concomitant with oceanic influences which give it particular climatic rhythms on the one hand, and on the other hand the north–west winds, meeting the Iberian chains (Spain) arriving dry in the north–west of Morocco. In addition, there is a simple succession of two climatic environments (cyclonic and anticyclonic), which have a remarkable influence on the inter-annual variability of the climate in Morocco (Driouech et al. 2021) and in particular in the LSB (Hakam et al. 2022b).

The dominant influence of large-scale climate indices on the evolution of drought was slightly manifested in the LSB. Consistency analysis indicates a significant influence of climate indices (NAO and MO) on drought variability at the annual to multi-year (5-year) scale, particularly during years with drought conditions (Figure 5). Both NAO and MO were strongly influenced by the North–East Atlantic cyclonic

systems that force Mediterranean cyclogenesis (Zeroual, Assani and Meddi 2017), inducing a strong correlation between them (Criado-Aldeanueva, Soto-Navarro and García-Lafuente 2014). The OM can be defined as an oscillation of sea level pressure anomalies (SLP) in the central and western Mediterranean, an important source of cyclogenesis. As the occurrence of these cyclones is partly related to the activity of NAO–governed North Atlantic fronts, a strong correlation can be expected (Criado-Aldeanueva and Soto-Navarro 2020). For example, Angulo-Martínez and Beguería (2012) found that the erosive force of precipitation in the Ebro Basin (NE Spain) is strongest during negative phases of the NAO and OM. It is weaker during positive phases.

The statistical analysis is highly dependent on the observational (in–situ) data, such as the duration of observation, authentic source, spatial density and critical criteria used for the analysis, trends and periodicity. In addition, the analysis of global and regional climate models could provide physical dynamics of climate change and improve the reliability of the analysis results.

5 References

Abramowitz, M., Stegun, I. A. 1965: Handbook of mathematical functions. New York.

Acharki, S., Amharref, M., El Halimi, R., Bernoussi, A.-S. 2019: Assessment by statistical approach of climate change impact on water resources: Application to the Gharb perimeter (Morocco). Journal of Water Science 32-3. DOI: https://doi.org/10.7202/1067310ar

Agence du Bassin Hydraulique de Sebou. 2010: Evènements hydro-pluviométriques dans le bassin du Sebou 2009–2010. Maroc.

Ajlal, S., Agoutime, Z. 2021: Changements climatiques et leurs impacts dans la région du Gharb, Maroc. Journal of African Studies and River Nile Basin 3-11.

Angulo-Martínez M., Beguería S. 2012: Do atmospheric teleconnection patterns influence rainfall erosivity? A study of NAO, MO and WeMO in NE Spain, 1955–2006. Journal of Hydrology 450,168. DOI: https://doi.org/10.1016/j.jhydrol.2012.04.063

Bayissa, Y., Maskey, S., Tadesse, T., Van Andel, S. J., Moges, S., Van Griensven, A., Solomatine, D. 2018: Comparison of the performance of six drought indices in characterizing historical drought for the upper Blue Nile basin, Ethiopia. Geosciences 8-3. DOI: https://doi.org/10.3390/geosciences8030081

Beguería, S., Vicente-Serrano, S. M., Reig, F., Latorre, B. 2014: Standardized precipitation evapotranspiration index (SPEI) revisited: Parameter fitting, evapotranspiration models, tools, datasets and drought monitoring. International Journal of Climatology 34-10. DOI: https://doi.org/10.1002/joc.3887

Chang, X., Wang, B., Yan, Y., Hao, Y., Zhang, M. 2019: Characterizing effects of monsoons and climate teleconnections on precipitation in China using wavelet coherence and global coherence. Climate Dynamics 52. DOI: https://doi.org/10.1007/s00382-018-4439-1

Conte, M., Giuffrida, A., Tedesco, S. 1989: The Mediterranean Oscillation. Impact on precipitation and hydrology in Italy. Conference on Climate and Water. Helsinki.

Criado-Aldeanueva, F., Soto-Navarro, F. J., García-Lafuente, J. 2014: Large-scale atmospheric forcing influencing the long-term variability of Mediterranean heat and freshwater budgets: Climatic indices. Journal of Hydrometeorology 15-2. DOI: https://doi.org/10.1175/JHM-D-13-04.1

Criado-Aldeanueva, F., Soto-Navarro, J. 2020: Climatic indices over the Mediterranean Sea: A review. Applied Sciences 10-17. DOI: https://doi.org/10.3390/app10175790

Diani, K., Kacimi, I., Zemzami, M., Tabyaoui, H., Haghighi, A. T. 2019: Evaluation of meteorological drought using the Standardized Precipitation Index (SPI) in the High Ziz River basin, Morocco. Limnological Review 19-3. DOI: https://doi.org/10.2478/limre-2019-0011

Driouech, F. 2010: Distribution des précipitations hivernales sur le Maroc dans le cadre d'un changement climatique : descente d'échelle et incertitudes. Ph.D. thesis, University of Toulouse. Toulouse.

Driouech, F., Stafi, H., Khouakhi, A., Moutia, S., Badi, W., ElRhaz, K., Chehbouni, A. 2021: Recent observed country-wide climate trends in Morocco. International Journal of Climatology 41. DOI: https://doi.org/10.1002/joc.6734

El Jihad, M. -D., Peyrusaubes, D., El Bouzidi, A. 2014: Sécheresses saisonnières et changement climatique dans le Gharb (Maroc). Rur@lités 2014-4.

Gerstengarbe, F. -W., Werner, P. C. 1999: Estimation of the beginning and end of recurrent events within a climate regime. Climate Research 11-2. DOI: https://doi.org/10.3354/cr011097

Hakam, O., Baali, A., Ait Brahim, Y., El Kamel, T., Azennoud, K. 2022b: Regional and global teleconnections patterns governing rainfall in the Western Mediterranean: Case of the Lower Sebou Basin, North-West Morocco. Modeling Earth Systems and Environment. DOI: https://doi.org/10.1007/s40808-022-01425-3

Hakam, O., Baali, A., El Kamel, T., Ahouach, Y., Azennoud, K. 2022a: Comparative evaluation of precipitation-temperature based drought indices (DIs): A case study of Moroccan Lower Sebou basin. Kuwait Journal of Sciences 49-3. DOI: https://doi.org/10.48129/kjs.13911

Harbouze, R., Pellissier, J. -P., Rolland, J. -P., Khechimi, W. 2019: Rapport de synthèse sur l'agriculture au Maroc. Internet: https://hal.archives-ouvertes.fr/hal-02137637/document (14. 6. 2022).

Lamb, P.J., Peppler, R.A. 1987: North Atlantic Oscillation: Concept and an application. Bulletin of the American Meteorological Society 68-10. DOI: https://doi.org/10.1175/1520-0477(1987)068<1218:NAOCAA>2.0.CO;2

Linares, J. C., Camarero, J. J. 2012: From pattern to process: Linking intrinsic water-use efficiency to drought-induced forest decline. Global Change Biology 18-3. DOI: https://doi.org/10.1111/j.1365-2486.2011.02566.x

Liu, C., Yang, C., Yang, Q., Wang, J. 2021: Spatiotemporal drought analysis by the standardized precipitation index (SPI) and standardized precipitation evapotranspiration index (SPEI) in Sichuan Province, China. Scientific Reports 11. DOI: https://doi.org/10.1038/s41598-020-80527-3

Marchane, A., Jarlan, L., Boudhar, A., Tramblay, Y., Hanich, L. 2016: Linkages between snow cover, temperature and rainfall and the North Atlantic Oscillation over Morocco. Climate Research 69-3. DOI: https://doi.org/10.3354/cr01409

McGuire, A. D., Ruess, R. W., Lloyd, A., Yarie, J., Clein, J. S., Juday, G. P. 2010: Vulnerability of white spruce tree growth in interior Alaska in response to climate variability: Dendrochronological, demographic, and experimental perspectives. Canadian Journal of Forest Research 40-7. DOI: https://doi.org/10.1139/X09-206

McKee, T. B., Doesken, N. J., Kleist, J. 1993: The relationship of drought frequency and duration to time scales. Proceedings of the 8th Conference on Applied Climatology. Boston.

Ministry of Agriculture and Maritime Fisheries. 2020: Regional agricultural plan – Region of Gharb – Chrarda – Beni Hssen. Internet: https://www.ormvag.ma/PDF/Brochures/Plaquette PAR ORMVAG.pdf (14. 6. 2022).

Pyarali, K., Peng, J., Disse, M. Tuo, Y. 2022: Development and application of high resolution SPEI drought dataset for Central Asia. Scientific Data 9. DOI: https://doi.org/10.1038/s41597-022-01279-5

Regional Observatory of the Environment and Sustainable Development. 2014: Climate change in the region of Gharb, Chrarda and Beni Hssen. Internet: https://www.4c.ma (24. 12. 2021).

Šebenik, U., Brilly, M., Šraj, M. 2017: Drought analysis using the standardized precipitation index (SPI). Acta geographica Slovenica 57-1. DOI: https://doi.org/10.3986/AGS.729

Stagge, J. H., Tallaksen, L. M., Gudmundsson, L., Van Loon, A. F., Stahl, K. 2015: Candidate distributions for climatological drought indices (SPI and SPEI). International Journal of Climatology 35-13. DOI: https://doi.org/10.1002/joc.4267

Stigter, T. Y., Nunes, J. P., Pisani, B., Fakir, Y., Hugman, R., Li, Y., Tomé, S. et al. 2014: Comparative assessment of climate change and its impacts on three coastal aquifers in the Mediterranean. Regional Environmental Change 14. DOI: https://doi.org/10.1007/s10113-012-0377-3

Thornthwaite, C. W. 1984: An approach toward a rational classification of climate. Geographical Review 38-1. DOI: https://doi.org/10.2307/210739

Torrence, C., Webster, P. J. 1999: Interdecadal changes in the ENSO–monsoon system. Journal of Climate 12-8. DOI: https://doi.org/10.1175/1520-0442(1999)012<2679:ICITEM>2.0.CO;2

United Nations Office for Disaster Risk Reduction. 2021: Special report on drought 2021. Internet: https://www.undrr.org/publication/gar-special-report-drought-2021 (14. 6. 2022).

Vatter, J., Wagnitz, P., Hernandez, E. 2019: Drought risk. The global thirst for water in the era of climate crisis. Internet: https://d2ouvy59p0dg6k.cloudfront.net/downloads/drought_risk__wwf_.pdf (14. 6. 2022).

Vicente-Serrano, S. M., Beguería, S. 2016: Comment on 'candidate distributions for climatological drought indices (SPI and SPEI). International Journal of Climatology 36-4. DOI: https://doi.org/10.1002/joc.4474

Vicente-Serrano, S. M., Beguería, S., López-Moreno, J. I. 2010: A multiscalar drought index sensitive to global warming: The standardized precipitation evapotranspiration index. Journal of Climate 23-7. DOI: https://doi.org/10.1175/2009JCLI2909.1

Vicente-Serrano, S. M., Beguería, S., Lorenzo-Lacruz, J., Camarero, J. J., López-Moreno, J. I., Azorin-Molina, C., Revuelto, J. et al. 2012: Performance of drought indices for ecological, agricultural, and hydrological application. Earth Interactions 16-10. DOI: https://doi.org/10.1175/2012EI000434.1

Vicente-Serrano, S. M., Quiring, S. M., Peña-Gallardo, M., Yuan, S., Dominguez-Castro, F. 2020: A review of environmental droughts: Increased risk under global warming? Earth-Science Reviews 201. DOI: https://doi.org/10.1016/j.earscirev.2019.102953

Wilhite, D. 2006: Drought monitoring and early warning: Concepts, progress and future challenges. Internet: https://public.wmo.int/en/resources/library/drought-monitoring-and-early-warning-concepts-progress-and-future-challenges (14. 6. 2022).

Woillez, M. - N. 2019: Revue de littérature sur le changement climatique au Maroc: Obsrvations, projections et impacts. DOI: https://doi.org/10.3917/afd.woill.2019.01.0001

World Meteorological Organization. 2012: Standardized precipitation index. User guide. Internet: https://library.wmo.int/doc_num.php?explnum_id=7768 (14. 6. 2022).

Yevjevich, V. M. 1967: Objective approach to definitions and investigations of continental hydrologic droughts. Ph.D. thesis, Colorado State University. Colorado.

Yihdego, Y., Vaheddoost, B., Al-Weshah, R. A. 2019: Drought indices and indicators revisited. Arabian Journal of Geosciences 12-3. DOI: https://doi.org/10.1007/s12517-019-4237-z

Zamrane, Z., Mahé, G., Laftouhi, N.-E. 2021: Wavelet analysis of rainfall and runoff multidecadal time series on large river basins in western North Africa. Water 13-22. DOI: https://doi.org/10.3390/w13223243

Zeroual, A., Assani, A. A., Meddi, M. 2017: Combined analysis of temperature and rainfall variability as they relate to climate indices in northern Algeria over the 1972–2013 period. Hydrology Research 48-2. DOI: https://doi.org/10.2166/nh.2016.244